Surface exposure to sunlight stimulates CO_2 release from permafrost soil carbon in the Arctic

Rose M. Cory[a,1], Byron C. Crump[b], Jason A. Dobkowski[c], and George W. Kling[c]

[a]Environmental Sciences and Engineering, University of North Carolina, Chapel Hill, NC, 27599; [b]Horn Point Laboratory, University of Maryland, Cambridge, MD, 21613; and [c]Department of Ecology and Evolutionary Biology, University of Michigan, Ann Arbor, MI, 48109

Recent climate change has increased arctic soil temperatures and thawed large areas of permafrost, allowing for microbial respiration of previously frozen C. Furthermore, soil destabilization from melting ice has caused an increase in thermokarst failures that expose buried C and release dissolved organic C (DOC) to surface waters. Once exposed, the fate of this C is unknown but will depend on its reactivity to sunlight and microbial attack, and the light available at the surface. In this study we manipulated water released from areas of thermokarst activity to show that newly exposed DOC is >40% more susceptible to microbial conversion to CO_2 when exposed to UV light than when kept dark. When integrated over the water column of receiving rivers, this susceptibility translates to the light-stimulated bacterial activity being on average from 11% to 40% of the total areal activity in turbid versus DOC-colored rivers, respectively. The range of DOC lability to microbes seems to depend on prior light exposure, implying that sunlight may act as an amplification factor in the conversion of frozen C stores to C gases in the atmosphere.

carbon cycling | photochemistry | dissolved organic matter | bacterial community composition | stream

High-latitude soils currently store at least twice the carbon found in the atmosphere (1–3), and recent climate change has increased soil temperatures (4), deepened the active layer (5, 6), and thawed large areas of permafrost (7). Thawed soils allow for microbial respiration of previously frozen C and seem to increase the net loss of CO_2 to the atmosphere (8), further accentuating the debate on whether thawing of arctic soil C and release as greenhouse gases will create a positive feedback on global warming (9–11). Furthermore, recent increases in thermokarst failures (12) because of melting ice and soil subsidence (6) indicate that thawed soil C may not be processed in situ, but instead it will be mixed to the surface, exposed to light, and increasingly released as dissolved organic carbon (DOC) to surface waters (13, 14). Once exposed, the fate of this C is unknown but will depend on its reactivity to the combined effects of sunlight and microbial processing.

Sunlight has contrasting effects on how dissolved organic matter (DOM) is processed by bacteria; coupled photochemical plus biological processing of fresh DOM with little prior light exposure may convert up to 90% of the DOC to CO_2, whereas overexposure or previous degradation of DOM can reduce its lability to bacteria and inhibit conversion to CO_2 (15, 16). However, only two studies have examined these coupled processes in arctic freshwaters (17, 18), and because neither study characterized DOM originating in permafrost soils we cannot predict the vulnerability of now-frozen C to photobiological alteration when introduced to surface conditions. Transfers of C from soils to surface waters are especially strong in the Arctic (19), where C fluxes from surface waters to the atmosphere and from land to ocean could represent up to 40% of the net land–atmosphere carbon exchange in the Arctic, given a maximum flux of ~0.16 Pg $C \cdot y^{-1}$ and a net terrestrial sink of 0.4 ± 0.4 Pg $C \cdot y^{-1}$ (20). With every indication that increasing thermokarst activity will enhance the surface exposure of currently frozen C, predicting the fate of arctic C stores in a warming world may hinge on its photobiological response and whether DOC released from soils to surface waters is preferentially converted to CO_2 and released to the atmosphere or transported downstream to the ocean.

During 2010–2011 we analyzed water from 27 different locations representing undisturbed sites in addition to seven unique thermokarst failures near Toolik Lake, Alaska (Fig. S1). By definition, a thermokarst failure is generated when ice-rich, permanently frozen soils are thawed, the ice melts, and the soil collapses and either creates an erosional gully in the tundra or a detachment failure (landslide) if the slope is sufficient (6) (Fig. S2). Therefore, because thermokarst failures must be initiated by the melting of permafrost ice, water draining a failure contains permafrost C. The study sites represent glacial surfaces with ages from ~10 ka to ~2 Ma, as well as three major forms of thermokarst failures including slumps in preexisting stream channels (Toolik River, Valley of Thermokarsts), thermo-erosional gullies (I-Minus, Huryn), and streams and pools formed by headwall glacial thaw slumps (Lake 395, Gunsight Mountain, Horn Lake). Reference streams and lakes were sampled either upstream or adjacent to the thermokarst failure sites. Water from all sites was analyzed optically for colored and fluorescent dissolved organic matter (CDOM and FDOM). DOM photobleaching was measured, and at six thermokarst and reference sites water was manipulated by exposure to sunlight followed by measurements of bacterial production and respiration in bioassay experiments. The water column light field was measured in the Kuparuk and Sagavanirktok Rivers to translate the susceptibility of thermokarst DOC to photoexposure into rates of light-stimulated versus dark bacterial production under natural conditions.

Results and Discussion

Thermokarst-impacted water generally had greater concentrations of DOC, CDOM, and FDOM compared with undisturbed waters (e.g., mean DOC 3,020 ± 1,130 impacted versus 830 ±110 SE micromolar reference; Table 1), and DOC concentrations were positively correlated with levels of CDOM (a_{300}, Pearson's r = 0.70, P = 0.001, n = 25). Overall, the water from thermokarst sites had lower CDOM per unit DOC (specific UV absorbance, $SUVA_{254}$) and a higher fluorescence index (FI) than the reference sites, which is the opposite of what was expected given that terrestrially derived DOM from plants and soils typically has higher SUVA and lower FI than do surface waters (17, 21). However, these thermokarst disturbances penetrated well beyond the upper 20–40 cm of organic mat (roughly

ECOLOGY

Table 1. DOM characteristics in thermokarst and reference waters

Characteristic	Mean ± SE		P value
	Reference	Impacted	
DOC (μM)	928 ± 72	3,019 ± 1,660	0.03
TDN (μM)	25.2 ± 1.8	198.8 ± 128.6	<0.01
C/N (M)	36.8 ± 1.1	25.8 ± 4.8	0.01
a_{300} (m^{-1})	51.6 ± 5.3	69.3 ± 16.0	ns
SUVA$_{254}$	3.5 ± 0.1	2.5 ± 0.5	0.01
S$_R$	0.84 ± 0.04	0.94 ± 0.07	ns
FI	1.38 ± 0.02	1.46 ± 0.02	0.05

Thermokarst site waters had consistently different DOM character than reference sites for DOC, total dissolved nitrogen (TDN), C/N molar ratio, a_{300} (m^{-1}), and SUVA$_{254}$ [m^{-1} (mg C·L)$^{-1}$]; slope coefficient ratio (S$_R$) and fluorescence index (FI) are dimensionless numbers. P values given for single-factor ANOVA comparisons (data distributions normalized by log transformation) between thermokarst-impacted ($n = 7$) versus reference ($n = 17$) sites for each variable; error bars represent the SEM. ns, not significant at $P = 0.1$ or lower. Data from Table S1.

equivalent to the summer active layer thaw depth) and into the underlying mineral soil (Fig. S2). Higher DOC levels at thermokarst sites are consistent with high C content found in arctic mineral soils (2), but unlike reference waters draining the overlying organic mat, DOM from mineral soil had significantly lower values of SUVA$_{254}$ and lower C/N ratios (Table 1). Lower SUVA$_{254}$ and C/N ratios are consistent with studies of mineral versus organic soils in other regions (21) and indicate that the chemical and optical character of water draining thermokarst disturbances is strongly influenced by deeper, previously frozen mineral soils.

Sunlight exposure stimulates the light-absorbing, chromophoric fraction of DOM and promotes photobleaching and degradation of the wider DOM pool to yield CO_2 or CO, low-molecular-weight compounds, or incompletely oxidized, more recalcitrant material (22, 23). As expected from previous work (17, 24), when exposed to light all samples showed a loss of CDOM and FDOM and a change in DOM character with increases in slope coefficient ratio (S$_R$) and decreases in FI (Table S1). Overall, photobleaching (loss of CDOM with light exposure) normalized to the moles of photons absorbed varied tenfold across all sites (Table S2), and there was on average higher photobleaching at thermokarst sites than at their respective reference sites [926 ± 145 versus 551 ±119 SE m^{-1} (mol photon·m^{-2})$^{-1}$, $P = 0.09$, $n = 7$, one-tailed t test on log-transformed data; data from Table S2]. This relationship of higher photobleaching in the thermokarst waters with lower SUVA$_{254}$ values than in reference waters (Table 1) is the opposite of what was expected, because lower SUVA$_{254}$ values indicate lower aromatic C content and thus lower potential for photodestruction of aromatic C (17). In addition, photobleaching was uncorrelated with the amounts of CDOM ($a_{CDOM\lambda}$) or aromatic C (SUVA$_{254}$) initially present in either reference or thermokarst samples. Our interpretation of these results is that it is misleading or at best too simplistic to assume the susceptibility of DOM to photochemical reactions is mainly a function of the amounts of CDOM, DOC, or aromatic C present. Clearly other characteristics of the DOM in thermokarst waters are controlling its susceptibility to photobleaching, and our results suggest the potential for greater alteration of thermokarst-derived DOM when exposed to sunlight compared with DOM in resident surface waters.

The net effect of all photochemical alterations was to stimulate the bacterial degradation of new DOM released from thermokarst failures, whereas in reference water these alterations tended to inhibit bacterial production and thus degradation of DOM (Fig. 1). On average, bacterial production (BProd) was increased

by 46.8 ± 2.6 (SE) % in thermokarst waters and decreased by −13.7 ± 1.2 (SE) % in reference waters following photoexposure relative to dark controls. Inhibition of bacterial production by light is often found in natural waters (15), including arctic soil and surface waters (18). These differences between thermokarst and reference sites and between light and dark were unrelated to the amount of DOC available as substrate for the bacteria. For example, dividing BProd by DOC concentration did not alter the result of BProd stimulation in thermokarst waters and inhibition in reference waters, and BProd and BProd normalized to DOC concentration (μg C·L^{-1}·d^{-1} per mg C-DOC·L^{-1}) were strongly correlated (Pearson $r = 0.97$, $P < 0.001$, $n = 22$; Table S3). Bacterial respiration (BResp) measured as O_2 loss on a mass spectrometer showed a similar pattern of stimulated activity in the thermokarst waters and inhibition in the reference waters, and the relationship between BProd and BResp had an $R^2 = 0.86$ (ordinary least squares, $n = 14$; Table S3). Assuming a respiratory quotient of 1.0 (mol O_2 consumed to mol CO_2 produced), the CO_2 produced by photoexposed thermokarst water exceeded that produced in the dark by 42%, 1.27 ± 0.51 versus 0.73 ± 0.23 (SE) μmol CO_2·L^{-1}·d^{-1}, respectively (one-tailed t test, $P = 0.037$, $n = 11$, log-transformed data). The mean CO_2 production for all light and dark samples in reference waters was 0.75 μmol CO_2·L^{-1}·d^{-1}.

The photoamplification of bacterial production in thermokarst waters is correlated with the extent of photobleaching (Fig. 2). For reference sites photobleaching was variable but relatively low, and light often inhibited bacterial activity, as shown by a negative percent difference between light minus dark treatments (Fig. 1). However, for the thermokarst sites the photostimulation of bacterial activity was positively related to photobleaching ($R^2 = 0.72$; Fig. 2), indicating that progressive degradation of DOM initiated by light absorption provides bacteria with more labile compounds, augmenting the coupled photobiological degradation of newly exposed organic matter.

To compare the bacterial response to phototransformed DOM among samples, we related the cumulative production of bacterial C stimulated by photo-produced DOM (taken as the difference in BProd between light minus dark regrowth treatments) to the number of photons absorbed during exposure of DOM to light. This apparent quantum yield for photo-stimulated bacterial production ($\Phi_{pbp,\lambda=350\ nm}$) describes how much bacterial biomass (micromoles of C) was gained per unit of solar radiation absorbed by CDOM (moles of photons). Calculated Φ_{pbp} spanned
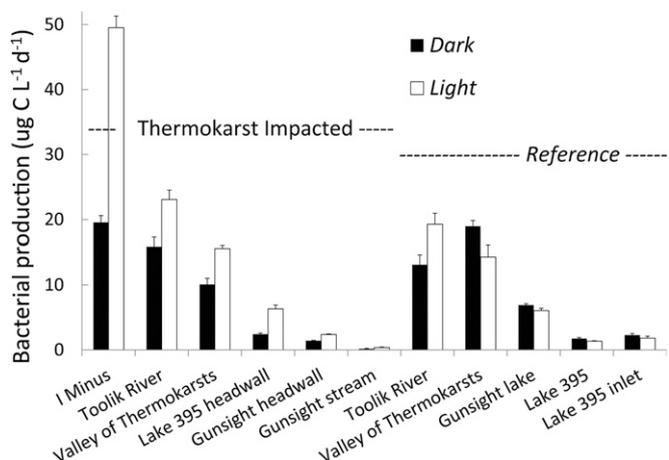

Fig. 1. In thermokarst impacted sites (*Left*), water exposed to natural sunlight stimulated bacterial activity by 46.8% (white versus black bars), whereas in corresponding reference sites the mean response was to decrease bacterial activity by −13.7% (single-factor ANOVA, $P = 0.0008$, $n = 11$, SE of three replicate samples for each bar for each site are shown).
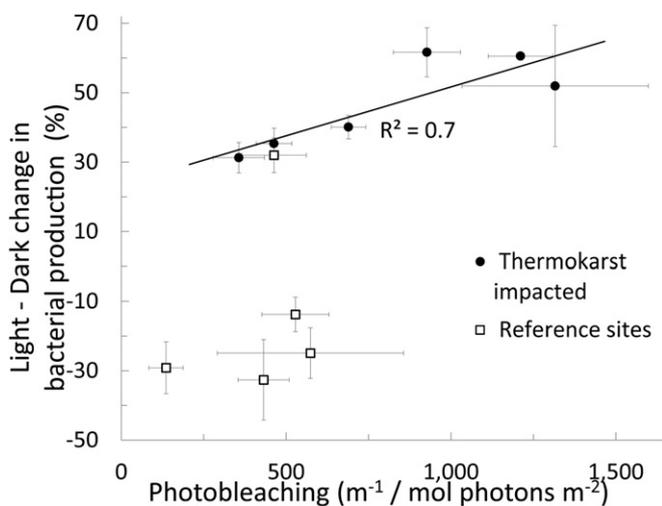
Cory et al.

Fig. 2. Percent difference between bacterial activity grown in light-exposed versus dark water plotted against the normalized moles of photons absorbed (photobleaching, integrated from 305 to 395 nm) in each thermokarst sample and its adjacent reference site. This illustrates that the extent of photobleaching controls the amplification of bacterial activity by light. SE bars are from three replicates for each sample or treatment; some error bars are hidden by the symbol. Ordinary least squares regression of percent change in bacterial activity versus photobleaching, $R^2 = 0.72$, $n = 6$, $P = 0.03$.

an order of magnitude for samples with a positive effect of light on bacterial production (Table S2 and Fig. 1) and overlapped the only other values previously reported (25). DOM with little previous exposure to sunlight should have the greatest yield of photo-products capable of stimulating bacterial production, and we used water temperature at the time of sampling to indicate proximity to deeper, frozen soils where the water would have low or no prior light exposure. The waters collected from active thermokarst failures all had colder temperatures, and despite sample collection over 2 yr with differing

weather conditions there was a strong inverse relationship between Φ_{pbp} and water temperature ($R^2 = 0.93$, $n = 4$, $P = 0.03$; data in Tables S1 and S2).

Several studies have shown that shifts in environmental conditions such as DOC concentration or lability drive shifts in bacterial community composition (26, 27). In turn, activity levels depend on species composition (28). Based on phylogenetic analysis of bacterial DNA from experiments for two thermokarst and one reference site, the difference in bacterial community composition between light and dark treatments was greatest for the thermokarst sample (I-Minus) with the highest apparent quantum yield, Φ_{pbp} (Fig. 3). Two other sites, Toolik River thermokarst and Toolik River reference, had much lower Φ_{pbp} and 2.6- to 3.4-fold lower photobleaching and showed essentially no change in bacterial community composition when bacteria were grown on DOM that was photo-exposed (Fig. 3). Because shifts in bacterial community composition are related to the degree of change in bacterial substrates (29), these results support the idea that photobleaching and quantum yield of stimulated bacterial production are proxies for total photochemical transformations of DOM; increased photo-transformation alters DOM chemistry relative to the dark control, which in turn drives and supports shifts in bacterial species and activity. This result also suggests that natural bacterial communities in thermokarst-disturbed waters have the genetic and metabolic capacity to process deep soil C when it is exposed to surface conditions.

Given that photochemical alteration of DOM in these arctic surface waters occurs on time scales similar to DOM transit in the same waters (17), and that microbial growth and processing (population doubling times) can be as fast as water transit times (30), the ultimate fate of deep, frozen soil C will be affected by coupled photobiological processing, by the available light field in streams that receive thermokarst drainage, and eventually by the landscape configuration of lakes and streams as they modify the DOM residence time and its total UV exposure. We measured the available light field in two rivers near Toolik (Fig. S3) and calculated the potential importance of light-stimulated bacterial production from thermokarst water DOM compared with the
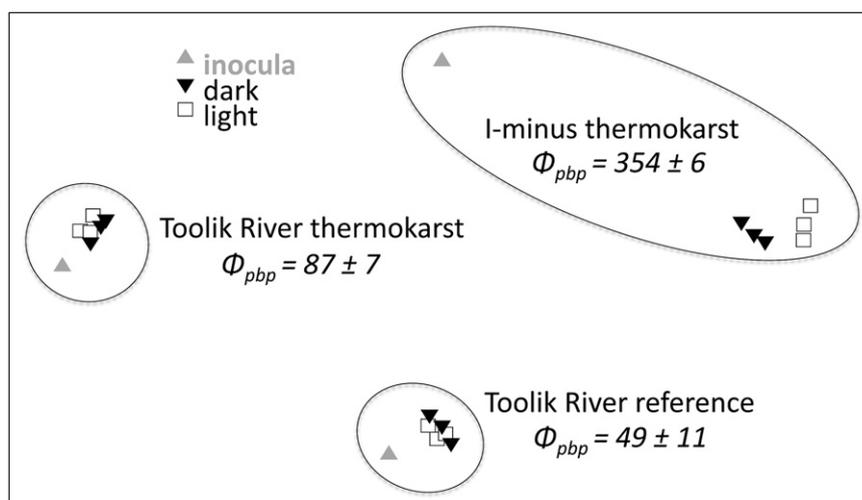
Fig. 3. Bacterial community composition for three sites showing the initial inoculum for regrowth experiments (gray triangle), the final dark treatment (black inverted triangle), and the final light treatment (open square) plotted using multidimensional scaling (MDS, 2D stress of analysis = 0.03). The sites had different bacterial community compositions (shown by distances between sites on the plot), and each community shifted in species composition between the original (inoculum) and the final light or dark treatments after 6 d [shifts from the inoculum effectively control for the "experiment bias" (26, 28)]. These shifts illustrate that the bacterial community composition is related to quantum yield of photoproduct-supported bacterial activity. The magnitude of shift between light and dark treatments was greatest for the I-Minus thermokarst site, which had the highest apparent quantum yield, Φ_{pbp} (μmol C/mol photon) of all samples and much greater photobleaching (1,211 ± 98) than Toolik River thermokarst (357 ± 78) or Toolik River reference (463 ± 76) SE [m^{-1}/(mol photons m^{-2})], Table S2).

dark bacterial production in reference surface water DOM under field conditions. Despite the colored nature of surface waters, UV light penetration was sufficient to reach the stream bottom under all conditions in the Kuparuk River (mean depth 0.5 m), representative of nearly all tundra streams where DOM is the main light absorption constituent ($a_{CDOM}/a_t = 1$), and under almost all conditions in the more turbid Sagavanirktok River (mean depth 0.7 m), representative of glacial and thermokarst outlet streams ($a_{CDOM}/a_t < 1$). The areal rate of photo-stimulated bacterial production is a product of the apparent quantum yield (pbp, Eq. **3**) and the rate of light absorption by DOM throughout the water column (Fig. S3 and Eq. **5**). We found that in the Kuparuk River the light-stimulated bacterial production was on average 39.3% of the total light plus dark bacterial production (239 ±57 SE μmol C·m^{-2}·d^{-1} light-stimulated, $n = 42$, versus 368 ±112 SE in the dark, $n = 5$; Fig. 4). The turbid conditions measured in the glacial-fed Sagavanirktok River reduced the contribution of photo-stimulated bacterial activity to an average of 11.1% (65 ±10 SE μmol C·m^{-2}·d^{-1} light-stimulated, $n = 108$, versus 515 ±157 SE in the dark, $n = 5$; Fig. 4). The variability in these estimates is due to sunny versus cloudy days, more versus less turbidity due to snowmelt and storms in the rivers, and to differences in quantum yield of different thermokarst waters. For example, on sunny days with I-Minus thermokarst water (lowest prior light exposure and highest Φ_{pbp}; Fig. 3 and Table S2), the areal light-stimulated bacterial activity was up to 3.8-fold higher than dark activity, and even in the turbid Sagavanirktok River the areal light-stimulated activity comprised up to

half of the total bacterial activity. These contributions of photo-related processes would be even higher in typical tundra streams with shallower water columns than those found in these two largest rivers in the area (Kuparuk and Sagavanirktok), and thus our conclusion is that the total degradation of thermokarst DOM is and will be substantially greater under sunlight conditions than under dark-only conditions.

Although no estimates exist for what percentage of now-frozen C will be released to the surface as the Arctic warms, the alteration and fate of this C will depend on its susceptibility to coupled photobiological processing and the available light. Our results suggest that photostimulation will rapidly (days to months) increase conversion to CO_2 by an additional 40% or more in thawed and released C compared with that remaining in the dark, and that photo-stimulated bacterial use of this C in natural streams may equal or exceed its degradation in the dark alone.

Materials and Methods

Water Chemistry. Temperature, pH, and conductivity were measured in the field. DOC and total dissolved nitrogen were measured in samples filtered in the field (GF/F filters; Whatman) and preserved with 6 M HCl and kept cold and dark until analysis on a Shimadzu TOC-V analyzer.

CDOM and FDOM. UV-Vis absorbance and fluorescence excitation–emission spectra were analyzed on GF/F filtered water in the field on an Ocean Optics USB 4000 and Horiba Fluoromax-4, respectively (23). The spectral coefficient S_R was calculated (24), and SUVA$_{254}$ was calculated as absorbance at 254 nm divided by path length (m) and DOC concentration (mg C·L^{-1}).

Bacterial Production, Respiration, and Community Composition. BProd was determined by measuring ^{14}C-labeled L-leucine incorporation into the cold trichloroacetic acid (TCA)-insoluble fraction of macromolecules in two or three subsamples and one TCA-killed control incubated in 10-mL plastic vials for 2–4 h at in situ temperatures in the dark (26). BResp was quantified as the loss of dissolved oxygen between three sample replicates and their three respective killed controls (1% HgCl$_2$), using a membrane inlet spectrometer (MIMS; Bay Instruments) in 12 mL-exetainer vials as a function of incubation time (23). Bacterial efficiency [BProd/(BProd + BResp)] was 33.4% ± 5.3 (SE) for the dark and 36.1% ± 5.4 (SE) for the light samples, similar to values found in other humic lakes (e.g., 38% found in ref. 31). DNA samples were collected on 0.2-μm Sterivex-GP filters (Millipore), fixed with 1 mL of DNA extraction buffer, and stored at −80 °C, and DNA was extracted (26) and PCR-amplified using bacteria-specific 16S ribosomal RNA gene primers for the V3 region. PCR products were separated on a denaturing gradient gel electrophoresis (DGGE) gel, and banding patterns were analyzed (32) except that PCR was performed in 50-μL reactions [1× PCR buffer (Qiagen), 1.5 mM MgCl$_2$, 0.2 mM deoxynucleoside triphosphates (dNTPs), 0.25 μM primers, 0.4 μg/μL BSA (BSA), 1× Q-Solution (Qiagen), and 0.025 U/μL TopTaq DNA polymerase (Qiagen)]. DGGE banding patterns were analyzed with Gelcompar-II software (Applied Maths), and similarity matrices and multidimensional scaling diagrams were generated in PRIMER v6 (32).

Photobiological Experimental Design. Triplicate GF/F filtered water samples placed in UV-transparent Whirlpak bags were exposed to simulated (40-W BL350 fluorescent black light tubes) or natural sunlight at Toolik Field Station for 12–15 h alongside triplicate foil-wrapped Whirlpak bags as dark controls. Sample photoexposure ranged from 1.85 to 2.94 moles of photons, and there was no relationship between moles of photons available and bacterial production or BProd percentage difference between light and dark values. After exposure to light, subsamples were analyzed for CDOM and FDOM as described above, and each light-exposed or dark-control replicate was filtered through 0.2-μm Sterivex filters, dispensed into amber HDPE incubation bottles, and inoculated with a natural bacterial community (equivalent to 20% of the sample volume). Bacterial inocula were prepared from each site by GF/C filtering fresh, whole water immediately following sample collection in the field. Bacterial regrowth incubations were carried out in the dark in an environmental chamber near the temperature of field samples for 5 to 7 d. Subsamples from the incubation bottles were taken at initial and final times for BProd, CDOM, and FDOM analyses to calculate time-integrated BProd and shifts in CDOM and FDOM. At the end of the incubation, samples for bacterial production, respiration, and CDOM/FDOM analysis were "killed" by addition of TCA, mercuric chloride, or GF/F filtration, respectively.
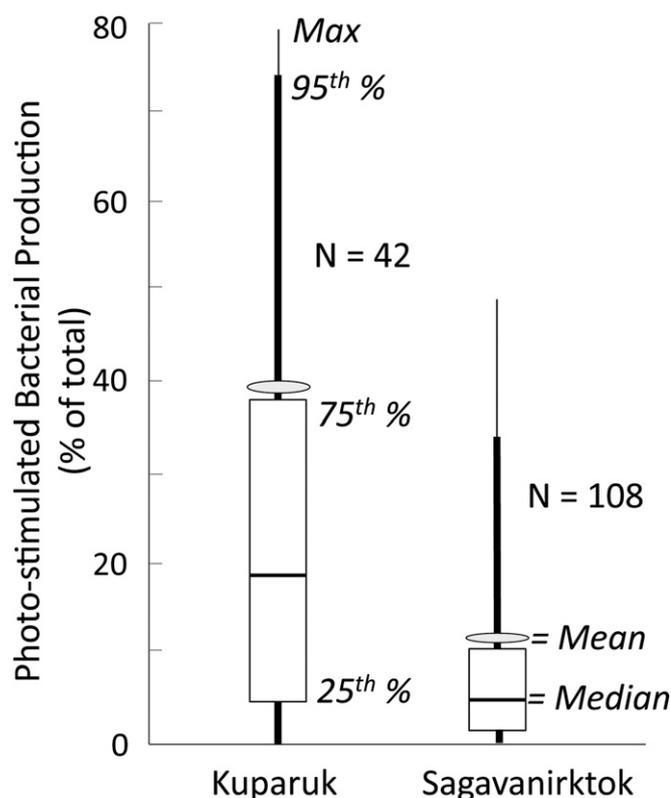

Fig. 4. Estimates of light-stimulated bacterial production integrated over the entire water column (areal) as a percentage of total light plus dark bacterial production in the Kuparuk and Sagavanirktok Rivers (*Materials and Methods*). Distributions of mean, median, minimum, maximum, 5th, 25th, 75th, and 95th percentiles were generated by the natural variation in measured surface irradiance, extinction of irradiance with depth (Fig. S3), and apparent quantum yields (Φ_{pbp}, μmol C/mol photon) in thermokarst water at six study sites (Table S2); Kuparuk $n = 42$, Sagavanirktok $n = 108$ combinations.

Photochemistry. We had two objectives in our photochemical studies: (*i*) to compare the susceptibility of DOM from thermokarst failures versus reference waters to photodegradation and (*ii*) to estimate the potential whole water column rates of photoproduction of DOM labile to bacteria. To compare the susceptibility of DOM to photodegradation, we calculated the apparent quantum yield of photobleaching and the apparent quantum yield of photo-produced DOM labile to bacteria. Apparent quantum yields are the moles of product (e.g., loss of chromophores in photobleaching, or photo-produced labile DOM) per moles of photons absorbed by the CDOM, and they allow for comparisons of photo-product yield during the exposure period by accounting for initial differences in CDOM among samples.

Photobleaching was calculated as the integral of the loss of CDOM absorption at each wavelength (λ) relative to the dark control normalized to the moles of photons absorbed by CDOM at the same wavelength, $Q_{a,\lambda}$, over the 12-h photoexposure (33):

$$Photobleaching_\lambda \left(m^{-1}\, mol^{-1}\, photons\, m^{-2} \right) = \int_{\lambda_{min}}^{\lambda_{max}} \frac{a_{CDOM,light_\lambda} - a_{CDOM,dark_\lambda}}{Q_{a,\lambda}},$$ [1]

where $Q_{a,\lambda}$ is calculated as

$$Q_{a,\lambda} \left(mol\, photons\, m^{-2} \right) = \int_{\lambda_{min}}^{\lambda_{max}n} E_{0,\lambda} \left[1 - e^{(-a_{t,\lambda} L)} \right] \frac{a_{CDOM_\lambda}}{a_{t,\lambda}},$$ [2]

where $a_{CDOM,\lambda}$ is the Naperian absorption coefficient of CDOM (m^{-1}), a_{CDOM}/a_t is the ratio of absorption by CDOM to the total absorption (assumed to be 1 for filtered waters exposed to light), $E_{0,\lambda}$ is the moles of photons available (surface irradiance, moles photons·m^{-2}·nm^{-1}), and L is the path length (m) in the Whirlpak bag. In Eq. **2**, $E_{0,\lambda}$ was calculated as the sum of diffuse and direct irradiance from 305 to 395 nm at 12:00 PM (noon) local time at Toolik Lake (68.66 °N 149.38 °W) for each experiment date (National Center for Atmospheric Research website total UV calculator). $E_{0,\lambda}$ was normalized to peak maximum and multiplied by the fraction of the total measured UVB or UVA light at each wavelength (Yankee Environmental Systems UVB and UVA sensors collecting at 5-min intervals at Toolik Field Station) to generate a photon flux spectrum. $E_{0,\lambda}$ of simulated light was measured by a PUV radiometer (Biospherical, Inc.) at 305, 312, 320, 340, 380, and 395 nm; data were linearly interpolated to 1-nm increments before converting to a photon flux spectrum.

The rate of bacterial production supported by photo-produced DOM in our experimental vessel (pbp_0, photo-stimulated bacteria production in mol C·m^{-3}·d^{-1}, where $_0$ refers to surface values) is the measured light minus dark difference in bacterial production. This pbp_0 value is represented by the product of the apparent quantum yield for photo-stimulated bacterial production and the rate of photon absorption by CDOM (modified from refs. 33 and 34):

$$(light - dark)\, pbp_0 = \int_{305}^{395} \Phi_{pbp,\lambda} Q_{a,\lambda},$$ [3]

where $\Phi_{pbp,\lambda}$ is the apparent quantum yield for photo-stimulated bacterial production (mol C·mol^{-1} photons absorbed) and $Q_{a,\lambda}$ is the moles of photons absorbed by CDOM over the 12-h photoexposure as defined above (Eq. **2**). $\Phi_{pbp,\lambda}$ is thus a measure of the susceptibility of the DOM to photo-stimulated bacterial degradation and is used to test whether susceptibility was higher for thermokarst DOM than for resident DOM already present in surface waters. The apparent quantum yield $\Phi_{pbp,\lambda}$ is solved for by using the measured pbp_0 and the measured $Q_{a,\lambda}$ and assumes that $\Phi_{pbp,\lambda}$ increases exponentially with decreasing wavelength (25):

$$\Phi_{pbp,\lambda} = c\, e^{-d\lambda},$$ [4]

where c (mol C·mol^{-1} photons) and d (nm^{-1}) are positive parameters and λ is wavelength (nm). $\Phi_{pbp,\lambda}$ was calculated using an unconstrained nonlinear optimization (*fminsearch* function in Matlab 7.11.0) such that c and d gave the best fit between the measured and calculated pbp_0. This calculation assumes that each of the 91 1-nm spectral bands in the 305- to 395-nm range

contributed to the photoreactions with the weighting as specified by parameters c and d.

Our second objective was to estimate the potential areal rates of photo-stimulated bacterial production in a natural water column. This estimate uses the in situ measured rates of light absorption in the whole water column of two rivers (i.e., the moles of photons available in a natural setting) and the amount of light-stimulated bacterial production per moles of photons as calculated in Eq. **4** above. In other words, we multiplied the $\Phi_{pbp,\lambda}$ values by the surface light available and the rate of light absorption in a water column of depth z to estimate the rate of depth-integrated, whole water column photoproduction of labile DOM (pbp_{wc} in mol C·m^{-2}·d^{-1}) following (25)

$$pbp_{wc} = \int_{305}^{395} \Phi_{pbp,\lambda} \left[E_{0,\lambda} \left(1 - e^{(-K_{d,\lambda} z)} \right) \right] \frac{a_{CDOM_\lambda}}{a_{t,\lambda}}.$$ [5]

Four terms in Eq. **5** varied in nature: (*i*) the amount of surface light available, $E_{0,\lambda}$, which varied seasonally and between sunny and cloudy days, (*ii*) the attenuation of surface light with depth in the water column, $K_{d,\lambda}$, which varied with discharge-related changes in absorbing substances in a river (Fig. S3), (*iii*) the ratio of light absorption by CDOM to total light absorption, $a_{CDOM_\lambda}/a_{t,\lambda}$, which varied with discharge-related changes in dissolved versus particulate absorbing substances, and (*iv*) the apparent quantum yield, $\Phi_{pbp,\lambda}$, which varied across different thermokarst sites sampled (Table S2). We characterized the natural variation in the first three terms for each unique site and date sampled for the Kuparuk ($n = 7$) and Sagavanirktok ($n = 18$) Rivers during summers of 2011 and 2012. For each site and date we used the surface irradiance ($E_{0,\lambda}$) spectrum calculated from the Yankee Environmental Systems UV sensors and National Center for Atmospheric Research Tropospheric Ultraviolet and Visible Radiation Model (described above). The attenuation of surface irradiance with depth through the water column (diffuse attenuation coefficient $K_{d,\lambda}$, m^{-1}) was calculated using data from a compact optical profiling system (C-OPS; Biospherical, Inc.), which measures downwelling irradiance at six wavebands of UVB and UVA light (305, 313, 320, 340, 380, 395, and 412 nm); representative in situ light profiles are shown in Fig. S3. We estimated the fraction of light absorbed by CDOM ($a_{CDOM,\lambda}/a_{t,\lambda}$) as the ratio of $a_{CDOM,\lambda}$ measured from the filtered water sample on the spectrophotometer divided by $K_{d,\lambda}$; this ratio ranged from 1 at all wavelengths for the Kuparuk River with low particulate concentrations to as low as 0.15 under very turbid conditions in the Sagavanirktok River. Finally, the natural variation in the fourth term, $\Phi_{pbp,\lambda}$, was characterized by the range of values measured in the six thermokarst sites (Table S2).

In applying Eq. **5** we used an average water depth of 0.5 m in the Kuparuk River and a depth of 0.7 m in the larger Sagavanirktok River. Most streams near Toolik are much shallower than these two deepest rivers in the area, and thus these depth values are conservative in terms of the amount of light available for photochemistry integrated through the water column. We multiplied the measured light field for each site and date by the calculated $\Phi_{pbp,\lambda}$ for each of the six thermokarst waters tested to generate a range and mean of possible values of light-stimulated bacterial production in a natural river. Thus, we generated $n = 42$ values (six thermokarst waters and seven unique light profiles and surface light values) for the Kuparuk and $n = 108$ values for the Sagavanirktok. These areal rates of water column bacterial production supported by photoproduction of labile DOM were compared with an areal estimate of the dark bacterial production, which was generated by multiplying the measured volumetric rates of dark bacterial production (mol C·m^{-3}·d^{-1}) in the reference sites ($n = 6$) by the depth of the river water column (m). Note that there was no statistically significant difference in dark bacterial production between the reference and thermokarst sites. We assumed that the $\Phi_{pbp,\lambda}$ for each of the six thermokarst waters tested would not change upon dilution of this water into a receiving surface water, and thus these values comparing the areal rates of light-stimulated versus dark bacterial activity are independent of potential dilution factors or discharge rates in the rivers.

1. Zimov SA, Schuur EAG, Chapin FS, 3rd (2006) Climate change: Permafrost and the global carbon budget. *Science* 312(5780):1612–1613.

2. Ping CL, et al. (2008) High stocks of soil organic carbon in the North American Arctic region. *Nat Geosci* 1:615–619.

Cory et al.

ECOLOGY

3. Tarnocai C, et al. (2009) Soil organic carbon pools in the northern circumpolar permafrost region. *Global Biogeochem Cycles* 23:, 10.1029/2008GB003327.

4. Osterkamp TE, Romanovsky VE (1999) Evidence for warming and thawing of discontinuous permafrost in Alaska. *Permafrost Periglacial Processes* 10:17–37.

5. Brown JG, Hinkel KM, Nelson FE (2000) The Circumpolar Active Layer Monitoring (CALM) program: Research designs and initial results. *Polar Geography* 24:165–258.

6. Jorgenson MT, Shur YL, Pullman ER (2006) Abrupt increase in permafrost degradation in Arctic Alaska. *Geophys Res Lett* 33(2):, D22103, L02053, 10.1029/2005GL024960.

7. Zhang Y, Chen W, Riseborough DW (2006) Temporal and spatial changes of permafrost in Canada since the end of the Little Ice Age. *J Geophys Res* 111, D22103, 10.1029/2006JD007284.

8. Schuur EAG, et al. (2009) The effect of permafrost thaw on old carbon release and net carbon exchange from tundra. *Nature* 459(7246):556–559.

9. Serreze MC, Francis JA (2006) The arctic amplification debate. *Clim Change* 76:241–264.

10. Davidson EA, Janssens IA (2006) Temperature sensitivity of soil carbon decomposition and feedbacks to climate change. *Nature* 440(7081):165–173.

11. Schuur EAG, et al. (2008) Vulnerability of permafrost carbon to climate change: Implications for the global carbon cycle. *Bioscience* 58:701–714.

12. Rowland JC, et al. (2010) Arctic landscapes in transition: Responses to thawing permafrost. *Eos* 91:229–236.

13. Bowden WB, et al. (2008) Sediment and nutrient delivery from thermokarst features in the foothills of the North Slope, Alaska: Potential impacts on headwater stream ecosystems. *J Geophys Res* 113, G02026, 10.1029/2007JG000470.

14. Olefeldt D, Roulet NT (2012) Effects of permafrost and hydrology on the composition and transport of dissolved organic carbon in a subarctic peatland complex. *J Geophys Res* 117, g1, G01005, 10.1029/2011JG001819.

15. Moran MA, Sheldon WM, Zepp RG (2000) Carbon loss and optical property changes during long-term photochemical and biological degradation of estuarine dissolved organic matter. *Limnol Oceanogr* 45:1254–1264.

16. Vähätalo AV, Wetzel RG (2004) Photochemical and microbial decomposition of chromophoric dissolved organic matter during long (months-years) exposures. *Mar Chem* 89:313–326.

17. Cory RM, McKnight DM, Chin YP, Miller P, Jaros CL (2007) Chemical characteristics of fulvic acids from Arctic surface waters: Microbial contributions and photochemical transformations. *J Geophys Res Biogeosciences* 112, G04S51, 10.1029/2006JG000343.

18. Judd KE, Crump BC, Kling GW (2007) Bacterial responses in activity and community composition to photo-oxidation of dissolved organic matter from soil and surface waters. *Aquat Sci* 69:96–107.

19. Kling GW, Kipphut GW, Miller MC (1991) Arctic lakes and streams as gas conduits to the atmosphere: Implications for tundra carbon budgets. *Science* 251(4991):298–301.

20. McGuire AD, et al. (2009) Sensitivity of the carbon cycle in the Arctic to climate change. *Ecol Monogr* 79:523–555.

21. Cory RM, Green SA, Pregitzer KS (2004) Dissolved organic matter concentration and composition in the forests and streams of Olympic National Park, WA. *Biogeochemistry* 67:269–288.

22. Zafiriou OC, Joussotdubien J, Zepp RG, Zika RG (1984) Photochemistry of natural-waters. *Environ Sci Technol* 18:A358–A371.

23. Cory RM, et al. (2010) Singlet oxygen in the coupled photo and biochemical processing of dissolved organic matter. *Environ Sci Technol* 44:3683–3689.

24. Helms JR, et al. (2008) Absorption spectral slopes and slope ratios as indicators of molecular weight, source, and photobleaching of chromophoric dissolved organic matter. *Limnol Oceanogr* 53:955–969.

25. Vähätalo AV, Aarnos H, Hoikkala L, Lignell R (2011) Photochemical transformation of terrestrial dissolved organic matter supports hetero- and autotrophic production in coastal waters. *Mar Ecol Prog Ser* 423:1–14.

26. Crump BC, Kling GW, Bahr M, Hobbie JE (2003) Bacterioplankton community shifts in an arctic lake correlate with seasonal changes in organic matter source. *Appl Environ Microbiol* 69(4):2253–2268.

27. Jones SE, Newton RJ, McMahon KD (2009) Evidence for structuring of bacterial community composition by organic carbon source in temperate lakes. *Environ Microbiol* 11(9):2463–2472.

28. Judd KE, Crump BC, Kling GW (2006) Environmental drivers control ecosystem function in bacteria through changes in community composition. *Ecology* 87(8):2068–2079.

29. Glaeser SP, Grossart H-P, Glaeser J (2010) Singlet oxygen, a neglected but important environmental factor: Short-term and long-term effects on bacterioplankton composition in a humic lake. *Environ Microbiol* 12(12):3124–3136 10.1111/j.1462-2920.2010.02285.x.nvimi.

30. Crump BC, Adams HE, Hobbie JE, Kling GW (2007) Biogeography of bacterioplankton in lakes and streams of an Arctic tundra catchment. *Ecology* 88(6):1365–1378.

31. Vähätalo AV, Salonen K, Munster U, Jarvinen M, Wetzel RG (2003) Photochemical transformation of allochthonous organic matter provides bioavailable nutrients in a humic lake. *Arch Hydrobiol* 156:287–314.

32. Fortunato CS, Crump BC (2011) Bacterioplankton community variation across river to ocean environmental gradients. *Microb Ecol* 62(2):374–382.

33. Hu C, Muller-Karger FE, Zepp RG (2002) Absorbance, absorption coefficient, and apparent quantum yield: A comment on common ambiguity in the use of these optical concepts. *Limnol Oceanogr* 47:1261–1267.

34. Vähätalo AV, Salkinoja-Salonen M, Taalas P, Salonen K (2000) Spectrum of the quantum yield for photochemical mineralization of dissolved organic carbon in a humic lake. *Limnol Oceanogr* 45(3):664–676.